Title
Dodecaploid Xenopus longipes provides insight into the emergence of size scaling relationships during development

Journal
Current Biology, 33(7)

ISSN
0960-9822

Authors
Miller, Kelly E
Cadart, Clotilde
Heald, Rebecca

Publication Date
2023-04-01

DOI
10.1016/j.cub.2023.02.021

Current Biology

Report

Dodecaploid *Xenopus longipes* provides insight into the emergence of size scaling relationships during development

Highlights

- Dodecaploid *X. longipes* provides a model to examine effects of large genome size
- Early developmental timing is similar across species, despite different N/C ratios
- Genome to cell size scaling emerges at the swimming tadpole stage
- Subcellular structures possess distinct scaling regimes during development

Authors

Kelly E. Miller, Clotilde Cadart, Rebecca Heald

Correspondence

bheald@berkeley.edu

In brief

Miller et al. examine the development of frog species of varying genome and egg sizes and observe that embryogenesis is characterized by distinct scaling regimes at the cellular and subcellular levels. Developmental timing is similar, despite differing nuclear-cytoplasmic ratios, with genome to cell size scaling emerging at the tadpole stage.

Miller et al., 2023, Current Biology *33*, 1–10
April 10, 2023
https://doi.org/10.1016/j.cub.2023.02.021

CellPress

Current Biology

CellPress OPEN ACCESS

Report

Dodecaploid *Xenopus longipes* provides insight into the emergence of size scaling relationships during development

Kelly E. Miller,[1] Clotilde Cadart,[1] and Rebecca Heald[1,2,3,*]
[1]Department of Molecular and Cell Biology, University of California, Berkeley, Berkeley, CA 94720-3200, USA
[2]Twitter: @rebeccaheald
[3]Lead contact
*Correspondence: bheald@berkeley.edu
https://doi.org/10.1016/j.cub.2023.02.021

SUMMARY

Genome and cell size are strongly correlated across species[1–6] and influence physiological traits like developmental rate.[7–12] Although size scaling features such as the nuclear-cytoplasmic (N/C) ratio are precisely maintained in adult tissues,[13] it is unclear when during embryonic development size scaling relationships are established. Frogs of the genus *Xenopus* provide a model to investigate this question, since 29 extant *Xenopus* species vary in ploidy from 2 to 12 copies (N) of the ancestral frog genome, ranging from 20 to 108 chromosomes.[14,15] The most widely studied species, *X. laevis* (4N = 36) and *X. tropicalis* (2N = 20), scale at all levels, from body size to cellular and subcellular levels.[16] Paradoxically, the rare, critically endangered dodecaploid (12N = 108) *Xenopus longipes* (*X. longipes*) is a small frog.[15,17] We observed that despite some morphological differences, *X. longipes* and *X. laevis* embryogenesis occurred with similar timing, with genome to cell size scaling emerging at the swimming tadpole stage. Across the three species, cell size was determined primarily by egg size, whereas nuclear size correlated with genome size during embryogenesis, resulting in different N/C ratios in blastulae prior to gastrulation. At the subcellular level, nuclear size correlated more strongly with genome size, whereas mitotic spindle size scaled with cell size. Our cross-species study indicates that scaling of cell size to ploidy is not due to abrupt changes in cell division timing, that different size scaling regimes occur during embryogenesis, and that the developmental program of *Xenopus* is remarkably consistent across a wide range of genome and egg sizes.

RESULTS AND DISCUSSION

Xenopus longipes provides a model to examine the effects of large genome size

Interspecies comparisons of pipid frogs have provided a powerful approach to characterize scaling relationships and molecular mechanisms of size control.[16] Studies have focused mainly on allotetraploid *X. laevis* (6.35 pg of DNA per nucleus) and diploid *X. tropicalis* (3.6 pg of DNA per nucleus), which possess larger and smaller genome, egg, tadpole, and adult body sizes, respectively.[16,18] However, other related species vary widely in morphometrics and genome content, providing a means to investigate the influence of different size parameters on embryogenesis and potential evolutionary constraints. At one extreme is *Xenopus longipes* (*X. longipes*), a small frog endemic to a single high-altitude lake in Cameroon, Africa (Figure 1A), that possesses a dodecaploid genome (16 pg of DNA per nucleus), the largest in the *Xenopus* genus.[15,17,19] Its large feet, relative to body size, distinguishes it from other *Xenopus* species[15,20] (Figures 1B, S1A, and S2A). Despite its large genome, *X. longipes* eggs are slightly smaller than those of *X. laevis* at 1.1 mm in diameter (Figure 1C). We used recently developed husbandry techniques[17] to generate *X. longipes* embryos via natural matings (Figure 1A) and documented their development compared with *X. laevis* side-by-side at the same temperature (Figure 1D). Early development in *X. laevis* has been extensively characterized through metamorphosis, as 12 rapid and synchronous cleavage divisions generate thousands of individual blastomeres up to the midblastula transition (MBT) at Nieuwkoop-Faber stages 8–9, 5–7 h post fertilization (hpf).[21–23] *X. longipes* early development proceeded almost indistinguishably through the MBT but slowed down at neurulation (stage 13, ∼16 hpf). Whereas *X. laevis* embryos assumed a tail-bud shape with a clear head, a tail, and eye protrusions by ∼25 hpf, *X. longipes* embryos remained round, with a closed neural tube but notable lack of anatomical structures (Figure 1D; Video S1). Previous work has documented an inverse correlation between genome size and developmental rate in many organisms,[7,10] and studies in frogs indicated longer larval periods in species with larger genomes,[8,9,11,24] in some cases with a direct relationship between amphibian genome size and duration of mitotic and meiotic cell cycles.[1,25,26] However, our analysis revealed only minor changes in cell-cycle timing of early cleavage divisions (Figure 1E), and despite variation in morphology at the late neurula stage 21 (22.5 hpf), cell proliferation was not significantly different between the species (Figure S1C). Furthermore, the timing of blastopore closure, which signifies the end of

Please cite this article in press as: Miller et al., Dodecaploid *Xenopus longipes* provides insight into the emergence of size scaling relationships during development, Current Biology (2023), https://doi.org/10.1016/j.cub.2023.02.021

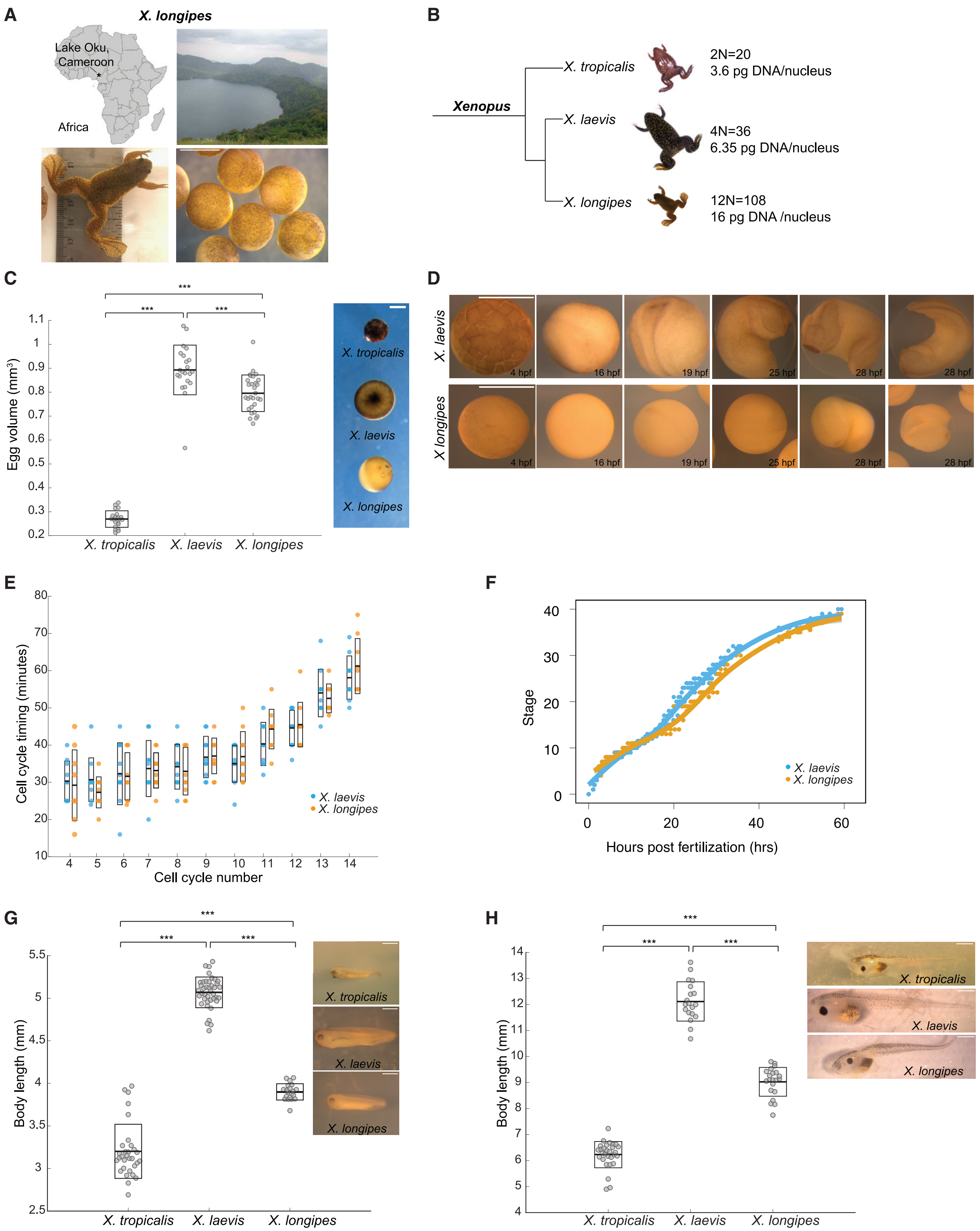

(legend on next page)

gastrulation,[27] was not delayed in *X. longipes* compared with *X. laevis* (Video S2). During later tail-bud stages 35–38 (∼50–60 hpf), the delay was much less evident (Figures 1F and 1G), and by the swimming tadpole stage (stage 48, 7 days post fertilization), there was little discernible difference between the species except for tadpole size (Figure 1H). Thus, while distinct morphological differences were clearly evident at certain developmental time points in *X. longipes*, the overall early developmental rate as compared with that of *X. laevis* was similar despite a nearly 3-fold difference in genome size.

Embryo cell size scales with egg size, not genome size, until late in development

In contrast to *X. laevis* and *X. tropicalis*, whose egg and adult body size scales with genome size, the large genome size yet relatively small egg and body size of *X. longipes* provides an extreme counterpoint. Across the tree of life, genome size correlates strongly and linearly with cell and nuclear size.[1–6] We confirmed this conserved relationship in adult frogs ranging nearly 5-fold in DNA content by measuring two cell types in four *Xenopus* species as well as *Hymenochirus boettgeri*, a related pipid frog. Both erythrocytes (which are nucleated in amphibians) and skin epithelial cells showed a strong, positive, and linear correlation among genome, cell, and nuclear sizes (Figures 2 and S2). Thus, despite their small size, relative to other *Xenopus* species, *X. longipes* adults possess large cells corresponding to their high ploidy.

Since *X. longipes* frogs possess fewer and larger cells than other *Xenopus* species, we hypothesized that genome to cell size scaling relationships were established during embryogenesis. However, consistent with the observation that cleavage division timing is similar across species, despite egg size and ploidy differences (Figure 1E), measurements over the course of development (Figures 3A–3C, S3A, and S3B) revealed no correlation between cell area and DNA content across species at stage 8. A weak correlation was observed at stages 21 and 36, and a linear relationship only at tadpole stage 48, 7 days post fertilization, when the unfed tadpoles were swimming and possessed well-developed organ and sensory systems[23] (Figures 3D and S3C). Instead, cell size varied with egg size throughout development and was strongly and linearly correlated from stages 21 through 36 and persisted through stage 48 (Figures 3E and S3D). By contrast, nuclear size correlated with genome size throughout development (Figures 3A, 3C, 3F, S3E, and S3F). Thus, egg size, rather than genome size, sets embryo cell size across these species, and genome to cell size scaling does not emerge until quite late in *Xenopus* development, while nuclear size continuously reflects genome size, consistent with a biophysical effect of DNA content on nuclear size.[29] Altogether, these results show that cell-cycle duration is not altered during embryogenesis to adjust to DNA amount, and they indicate that developmental timing is paramount to cell size scaling.

Embryogenesis is characterized by distinct size scaling regimes

Another way to evaluate changing size relationships across embryos of different *Xenopus* species is to characterize the nuclear-cytoplasmic (N/C) ratio, which is precisely maintained across eukaryotic organisms and cell types.[13] During development, a threshold N/C value is thought to contribute to the MBT when rapid cleavages abruptly cease; cycles of slow, asynchronous divisions begin; transcription of the zygotic genome ramps up dramatically; and when gastrulation and cell differentiation initiate.[22,33] MBT timing is influenced by both ploidy and cell size within a species.[22,34,35] However, measurements comparing embryos from the three different frogs around the time of MBT onset at stage 8 revealed that *X. laevis* cells possess a significantly lower N/C ratio than either *X. tropicalis* or *X. longipes* (Figures 3H and S3H). At this point in development, there was no correlation between genome size and cell size (Figure 3D). These findings suggest that the MBT occurs at different N/C ratios in different *Xenopus* species. Although RNA sequencing analysis during development has not yet been performed in *X. longipes*, zygotic genome activation (ZGA) appears to occur similarly in *X. tropicalis* and *X. laevis* embryos, with comparable expression patterns of key genes including beta catenin, Nodal2, Wnt3, Wnt4, BMP4, and BMP5, despite very different N/C ratios.[36,37] Current models suggest that titration of nuclear or chromatin factors,[38–40] as well as lengthened cell cycles,[41] and the capacity for nuclear import[42] can contribute to MBT and ZGA onset. Future experiments will elucidate whether maternal supplies are tuned according to egg and genome sizes so that a similar number of cleavage divisions lead to comparable MBT and zygotic transcription timing despite very different size metrics.

Figure 1. *X. longipes* morphometrics and development compared with other *Xenopus* species

(A) Map[28] and photograph[19] of Lake Oku in Cameroon, Africa, and images of *X. longipes* frog and blastula stage embryos. Scale bars, 1 mm.

(B) Phylogeny of *X. longipes* compared with *X. laevis* and *X. tropicalis*, with chromosome number and nuclear DNA content. See also Figure S1A for frog body length comparison.

(C) Calculated egg volume in *X. tropicalis*, *X. laevis*, and *X. longipes*. $n \geq 23$ eggs measured in each species. Scale bars, 0.5 mm.

(D) Images of development in *X. longipes* versus *X. laevis* at 23°C. hpf, hours post fertilization. Scale bars, 1 mm.

(E) Comparison of cell-cycle timing in animal pole cells of *X. longipes* versus *X. laevis* through the first 14 cleavage divisions. Each point represents the average timing for 3 individual cells. Thick line inside box indicates average time, and upper and lower box boundaries indicate ±SD. n = 3 cells from 10 total embryos analyzed per species from 3 separate clutches. $p > 0.5$ between species in each cell cycle, determined by two-tailed t test.

(F) Developmental time course in *X. longipes* versus *X. laevis* at 23°C, 0–62 hpf. n = 3 clutches analyzed for *X. laevis*, n = 2 for *X. longipes*, 1–3 replicates for each clutch. See also Videos S1 and S2 and Figure S1B for individual time points.

(G) Body length quantification of stage 36 tail-bud embryos in *X. tropicalis*, *X. laevis*, and *X. longipes*. $n \geq 20$ tadpoles from 3 clutches measured for each species. Scale bars, 1 mm.

(H) Body length quantification of stage 48 tadpoles in *X. tropicalis*, *X. laevis*, and *X. longipes*. $n \geq 20$ tadpoles from 3 separate clutches measured for each species. Scale bars, 1 mm.

For all boxplots, thick line inside box indicates average length, and upper and lower box boundaries indicate ±SD. ***$p < 0.001$, determined by two-tailed t test.

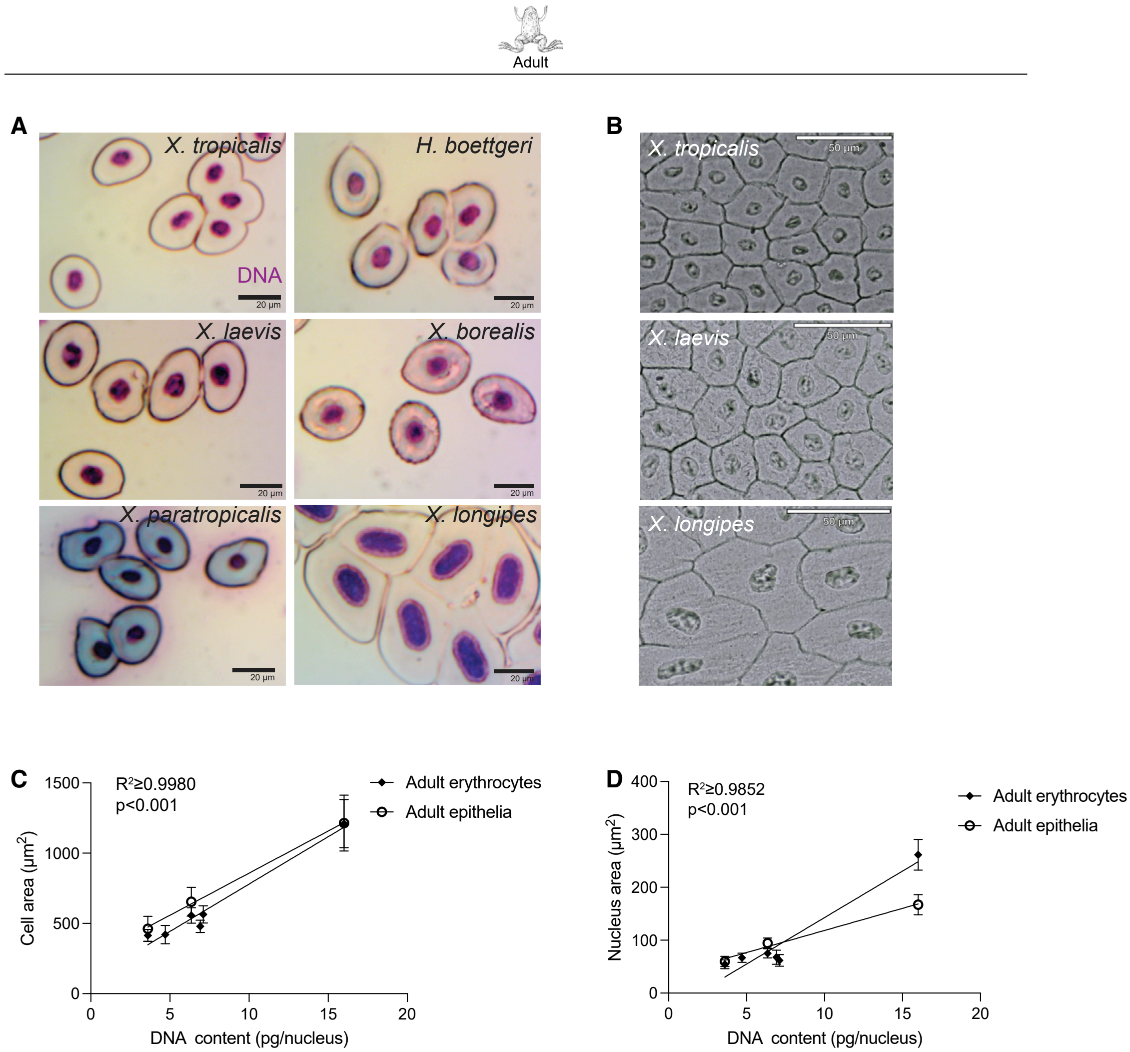

Figure 2. Scaling of cells and nuclei in adult pipid frog species

(A) Images of erythrocytes from 5 adult pipid frog species of varying ploidies. See Figure S2A for details about species, including DNA content. Scale bars, 20 μm.

(B) Images of adult epithelial cells from *X. tropicalis*, *X. laevis*, and *X. longipes*. Scale bars, 50 μm.

(C) Average cell cross-sectional area in adult erythrocytes and epithelia as a function of genome size for each frog species. Five pipid frog species are plotted for erythrocytes; *X. tropicalis*, *X. laevis*, and *X. longipes* are plotted for epithelial cells. $R^2 \geq 0.9980$ for both erythrocytes and epithelia. See Figures S2B and S2C for distributions and Figure S3C for correlation and slope coefficients of each trend line.

(D) Average nucleus cross-sectional area in adult erythrocytes and epithelia as a function of genome size for each frog species. Five pipid frog species are plotted for erythrocytes; *X. tropicalis*, *X. laevis*, and *X. longipes* are plotted for epithelial cells. $R^2 \geq 0.9852$ for both erythrocytes and epithelia. See Figures S2D and S2E for distributions and Figure S3F for correlation and slope coefficients of each trend line. For plots in (C) and (D), error bars indicate ±SD.

Beyond the MBT, between stages 21 and 36 of development that includes neurulation, the N/C ratio was similar in epithelial cells of all three *Xenopus* species (Figures 3H and S3H). During this period, rapid cell divisions ceased, and cell and nuclear sizes remained relatively constant (Figures 3B and 3C). Between stages 36 and 48, cell sizes again decreased, but now correlated with genome size, with *X. tropicalis* cells becoming smaller than *X. laevis* cells, which in turn were smaller than *X. longipes* cells, reflecting the emergence of genome to cell size scaling (Figures 3B and 3C). Nuclear sizes also decreased during this phase so that N/C ratios remained similar. However, embryo epithelial cells at stage 48 were smaller than adult skin cells across all three species, while nuclear sizes between adults and tadpoles were similar, leading to a significantly lower N/C ratio in adult epithelia, which was similar to that of adult erythrocytes (Figures 3B, 3C, 3H, and S3F). Therefore, whereas cell size and N/C ratio do not correlate with adult dimensions in swimming tadpoles, nuclear size does.

Altogether, these results indicate that distinct scaling regimes exist during development that may reflect the physiology of the embryo. In a first regime, embryos initially undergo rapid cleavage divisions that increase cell number and decrease cell size exponentially. Genome size during this regime appears to be irrelevant as cell-cycle timing of *X. longipes* was

Please cite this article in press as: Miller et al., Dodecaploid *Xenopus longipes* provides insight into the emergence of size scaling relationships during development, Current Biology (2023), https://doi.org/10.1016/j.cub.2023.02.021

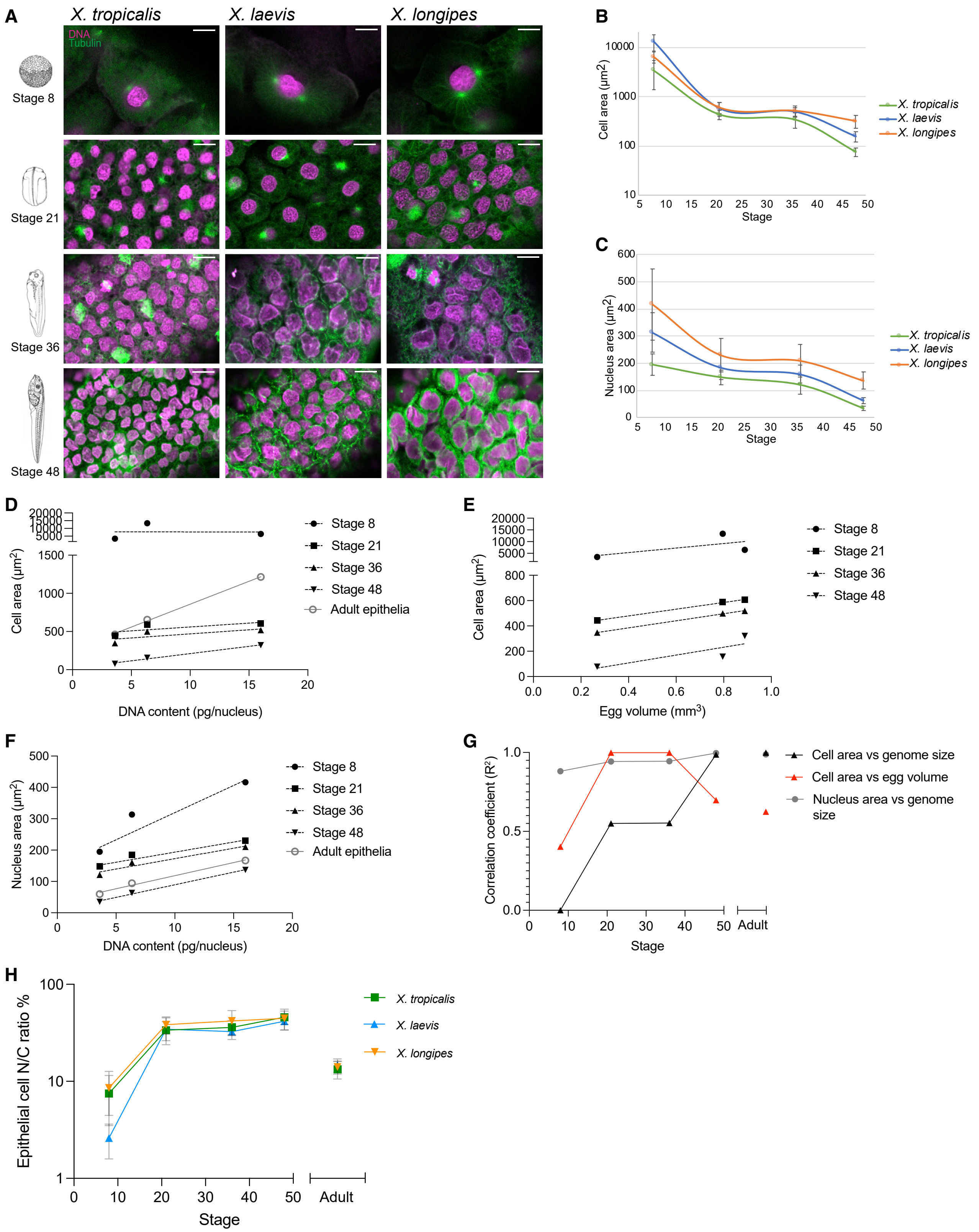

Figure 3. Scaling of cells and nuclei in *Xenopus* embryos
(A) Images of cells and nuclei in *X. tropicalis*, *X. laevis*, and *X. longipes* embryos, stages 8–48. Scale bars, 15 μm. Histone H3 staining indicates DNA.
(B) Average cross-sectional cell area during embryogenesis, y axis plotted in $\log_{10}$. See Figure S3B for distributions.

(legend continued on next page)

indistinguishable from that of *X. laevis* (Figure 1E). A second regime appears once a more consistent N/C ratio is established by neurulation at stage 21. During this period, complex cell movements are coordinated with differentiation, and cell divisions occur at a much lower frequency.[43] In a third regime, N/C ratios remain constant, but genome to cell size scaling is established by stage 48. Finally, larger, adult cell sizes and correspondingly lower N/C ratios emerge, which coincide with termination of the maternal program and the onset of tadpole feeding.

Embryo nuclei and spindle length scale with genome and cell size, respectively

Scaling of subcellular structures including the nucleus and the spindle to cell size has been characterized across *Xenopus* species and during early development, and molecular mechanisms were identified that coordinately scale both structures according to cell surface-to-volume ratio.[44] Although nuclear and spindle size has been documented extensively in *Xenopus* and other organisms in early cleaving embryos, prior to the MBT,[30–32,44,45] much less is known about subcellular scaling later in embryonic development, following the onset of zygotic transcription and morphogenesis. Our analysis revealed that although nuclear size correlated with cell size, as widely reported across species and cell types,[13] it was more highly correlated with genome size throughout development, starting as early as stage 8 (Figures 4A, 4B, S4A, and S4B). By contrast, we found that spindle length was only moderately correlated with genome size between stages 8 and 36, consistent with previous findings[32,45] (Figures 4C, 4D, S4B, and S4C). Instead, spindle length was strongly and linearly correlated with egg volume and cell size (Figures 4E–4G and S4D). Interestingly, spindle width (measured by the length of the metaphase plate) between stages 8 and 36 scaled similarly to nuclei, reaching a minimum length at stage 21 in all species and then remaining relatively constant (Figure S4E). Thus, nuclei and spindles possess distinct scaling properties through development, with nuclear size and spindle width influenced more by DNA content and spindle length by cell size.

In conclusion, the gradual emergence of genome to cell size scaling we observed in different *Xenopus* species during development reveals that the cell division cycle does not acutely adapt to genome size and that the transition to adult size scaling relationships (at least in skin epithelia) occurs after tadpoles begin feeding. Instead, egg size strongly influences cell size scaling during embryogenesis, highlighting the key role of maternally contributed components to the developmental program.[46] Interestingly, across *Xenopus* species, MBT and ZGA appear to occur with similar timing despite very different size metrics. Thus, over tens of millions of years of evolution, the basic developmental program in *Xenopus* frogs has remained robust to a 6-fold change in ploidy. Whether the observed developmental delay at neurulation and differences in *X. longipes* embryo morphogenesis result from its large genome is an open question, since cell sizes during this period are very similar to *X. laevis*, although nuclear sizes and N/C ratios were slightly greater in surface epithelia. Interestingly, a comparison of development in ten frog species showed a correlation between egg size and mode of gastrulation.[47] Further characterization of *X. longipes* embryogenesis and gene expression patterns will be informative in understanding the variation in morphogenesis with genome and cell size.

Our interspecies analysis provides an interesting comparison with classic work by Fankhauser showing that pentaploid salamanders are similar in size, possessing fewer and larger cells.[48] Additionally, *X. laevis* has been used for decades as a system in which ploidy can be manipulated to elucidate mechanisms underlying MBT and ZGA timing.[21,22,40] An important distinction is that previous work has focused primarily on acute ploidy changes within a species and not on comparing polyploid species that evolved and diverged tens of millions of years ago. Furthermore, until recently, evaluation of the impact of ploidy changes has largely been limited to early development.[49] Understanding mechanistic differences in acute vs. ancient ploidy alterations and overall effects of polyploidy on vertebrate physiology and development is a fascinating direction for future research.

Importantly, our analysis reveals that different scaling regimes operate during development across species. While the molecular mechanisms that underlie cell size scaling remain mysterious, future work will reveal how different size-dependent modalities emerge based on maternal resource allocation and temporal activation of growth signaling pathways, which in turn promise to shed light on when and how single-cell metabolic and biosynthesis properties, correlating with genome size,[50–52] affect tissue and whole-organism physiology. In addition to serving as an extreme case for investigating genome size effects on development and physiology, *X. longipes* also provides a powerful model

(C) Average cross-sectional nucleus area during embryogenesis. See Figure S3E for distributions.

For plots in (B) and (C), error bars indicate ±SD.

(D) To test the relationship between genome and cell size during development across species, we plotted average skin epithelial cell cross-sectional area in embryos and adults as a function of genome size in *X. tropicalis*, *X. laevis*, and *X. longipes* to generate regression lines. See Figure S3C for correlation and slope coefficients of each trend line.

(E) To test the relationship between egg volume and cell size during development across species, we plotted average skin epithelial cell cross-sectional cell area in *X. tropicalis*, *X. laevis*, and *X. longipes* through embryogenesis as function of egg volume to generate regression lines. See Figure S3D for correlation and slope coefficients of each trend line.

(F) To test the relationship between genome and nuclear size during development across species, we plotted average nucleus cross-sectional area in embryos and adults as a function of genome size in *X. tropicalis*, *X. laevis*, and *X. longipes* to generate regression lines. See Figure S3E for distributions and Figure S3F for correlation and slope coefficients of each trend line.

(G) Summary of correlation coefficients of cell or nucleus area vs. genome size or egg volume in embryos and adults from (D)–(F), plotted by developmental stage.

(H) To calculate N/C ratios through development across species, skin epithelial cell nuclear and cell volumes in embryos and adults of each species were extrapolated from cross-sectional area measurements,[30–32] and the ratio of nuclear to cell (N/C) volume was expressed as a percentage. Average values are plotted, y axis plotted in $\log_{10}$. Error bars indicate ±SD. See Figure S3G for validation that cross-sectional area measurements are not significantly different than volume measurements for calculating N/C ratios and Figure S3H for distribution of N/C ratios across species and developmental stages.

Please cite this article in press as: Miller et al., Dodecaploid *Xenopus longipes* provides insight into the emergence of size scaling relationships during development, Current Biology (2023), https://doi.org/10.1016/j.cub.2023.02.021

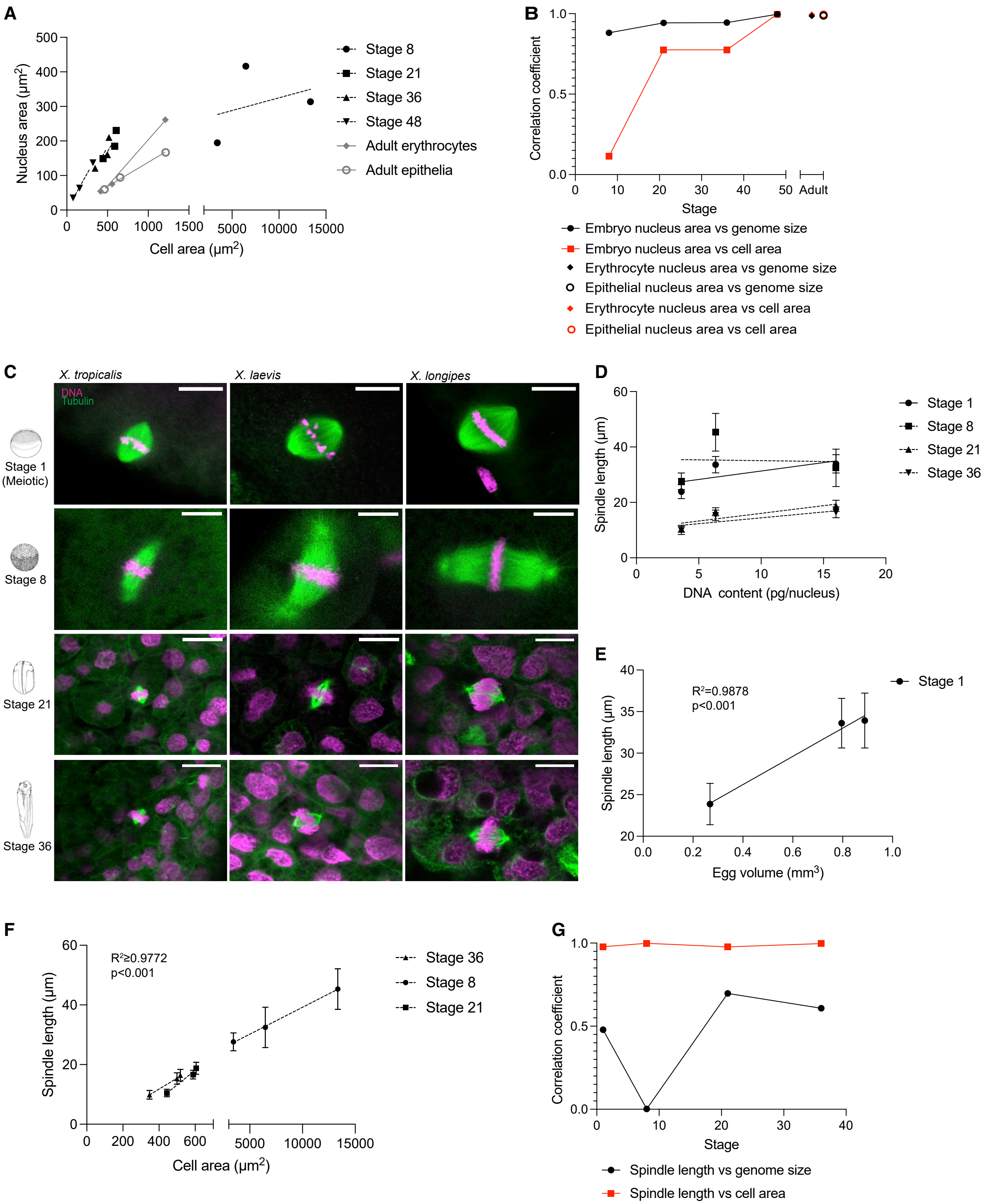

Figure 4. Subcellular scaling of nuclei and spindles through development

(A) Average cross-sectional nucleus area in *X. tropicalis*, *X. laevis*, and *X. longipes* embryos and adults, plotted as function of cell area.

(B) Summary of correlation coefficients of nucleus area versus genome size and cell area through development from Figure 3F and (A).

(legend continued on next page)

to study adaptations at the subcellular level. Whether and how 108 chromosomes impact nuclear and spindle organization, as well as the process of cell division, can be investigated in embryos, along with using powerful *in vitro* systems unique to *Xenopus*.[16]

STAR★METHODS

Detailed methods are provided in the online version of this paper and include the following:

- KEY RESOURCES TABLE
- RESOURCE AVAILABILITY
  - Lead contact
  - Materials availability
  - Data and code availability
- EXPERIMENTAL MODEL AND SUBJECT DETAILS
  - Chemicals
  - Frog care
- METHOD DETAILS
  - Erythrocyte preparation and measurements
  - Epithelial cell preparation and measurements
  - Natural mating of *X. longipes*
  - In vitro fertilization of *X. laevis*
  - Maintenance of *Xenopus* embryos
  - Imaging and measurement of egg diameters, developing embryos, and tadpoles
  - Live imaging
  - Cell Cycle Duration measurement
  - Embryo whole mount immunofluorescence
  - Confocal imaging and measurement of embryos, cells and nuclei after whole mount immunofluorescence
  - Egg volume and N/C ratio calculations
- QUANTIFICATION AND STATISTICAL ANALYSIS

SUPPLEMENTAL INFORMATION

Supplemental information can be found online at https://doi.org/10.1016/j.cub.2023.02.021.

ACKNOWLEDGMENTS

We thank Nicole Chaney and California Academy of Sciences for *X. longipes* frogs, as well as valuable husbandry advice; Ben Evans for helpful advice and *X. paratropicalis* blood smears; Jim Evans and Mike Fitzsimmons for dedicated and careful tadpole rearing; Scott Aposhian for initial measurements of erythrocytes; Harland lab members for assistance with ventral development movies; Helena Cantwell for critical reading of the manuscript; and members of the Heald lab, past and present, for helpful discussions and support with experiments. R.H. was supported by the NIH MIRA grant R35 GM118183 and the Flora Lamson Hewlett Chair.

AUTHOR CONTRIBUTIONS

Conceptualization, R.H., K.E.M., and C.C.; methodology, K.E.M. and C.C.; investigation, K.E.M. and C.C.; visualization, K.E.M. and C.C.; funding acquisition, R.H., K.E.M., and C.C.; supervision, R.H.; manuscript preparation, K.E.M., R.H., and C.C.

DECLARATION OF INTERESTS

The authors declare no competing interests.

INCLUSION AND DIVERSITY

We support inclusive, diverse, and equitable conduct of research.

Received: August 15, 2022
Revised: January 12, 2023
Accepted: February 6, 2023
Published: March 7, 2023

REFERENCES

1. Cavalier-Smith, T. (2005). Economy, speed and size matter: evolutionary forces driving nuclear genome miniaturization and expansion. Ann. Bot. *95*, 147–175. https://doi.org/10.1093/aob/mci010.
2. Sessions, S.K., and Larson, A. (1987). Developmental correlates of genome size in Plethodontid salamanders and their implications for genome evolution. Evolution *41*, 1239–1251. https://doi.org/10.1111/j.1558-5646.1987.tb02463.x.
3. Gillooly, J.F., Hein, A., and Damiani, R. (2015). Nuclear DNA content varies with cell size across human cell types. Cold Spring Harb. Perspect. Biol. *7*, a019091. https://doi.org/10.1101/cshperspect.a019091.
4. Gregory, T.R. (2001). Coincidence, coevolution, or causation? DNA content, cell size, and the C-value enigma. Biol. Rev. Camb. Philos. Soc. *76*, 65–101. https://doi.org/10.1111/j.1469-185X.2000.tb00059.x.
5. Turner, J.J., Ewald, J.C., and Skotheim, J.M. (2012). Cell size control in yeast. Curr. Biol. *22*, R350–R359. https://doi.org/10.1016/j.cub.2012.02.041.
6. Mirsky, A.E., and Ris, H. (1951). The desoxyrubonucleic acid content of animal cells and its evolutionary significance. J. Gen. Physiol. *34*, 451–462. https://doi.org/10.1085/jgp.34.4.451.
7. Goin, O.B., Goin, C.J., and Bachmann, K. (1968). DNA and amphibian life history. Copeia *1968*, 532. https://doi.org/10.2307/1442021.
8. Womack, M.C., Metz, M.J., and Hoke, K.L. (2019). Larger genomes linked to slower development and loss of late-developing traits. Am. Nat. *194*, 854–864. https://doi.org/10.1086/705897.
9. Camper, J.D., Ruedas, L.A., Waltham, J.W., and Dixon, J.R. (1993). The relationship of genome size with developmental rates and reproductive strategies in five families of Neotropical frogs. Life Sci. Adv. Genet. *12*, 79–87.
10. White, M.M., and McLaren, I.A. (2000). Copepod development rates in relation to genome size and 18S rDNA copy number. Genome *43*, 750–755. https://doi.org/10.1139/g00-048.
11. Oeldorf, E., Nishiokac, M., and Bachmann, K. (1978). Nuclear DNA amounts and developmental rate in holarctic anura. J. Zool. Syst. Evol. Res. *16*, 216–224. https://doi.org/10.1111/j.1439-0469.1978.tb00931.x.

(C) Images of meiotic and mitotic spindles in *X. tropicalis*, *X. laevis*, and *X. longipes* embryos, stage 1 (unfertilized meiotic) through stage 36. Scale bars, 20 μm. Histone H3 staining indicates DNA.
(D) Average spindle length plotted as a function of genome size in *X. tropicalis*, *X. laevis*, and *X. longipes* embryos. See Figure S4B for correlation and slope coefficients of each trend line and Figure S4C for distributions.
(E) Average egg spindle length (stage 1, meiotic) plotted as a function of egg volume. See Figure S4C for distribution.
(F) Average spindle length plotted as a function of cell area in *X. tropicalis*, *X. laevis*, and *X. longipes* embryos. See Figure S4C for distribution and Figure S4D for correlation and slope coefficients of each trend line.
(G) Summary of correlation coefficients of spindle length vs. genome size or cell area through development from (D)–(F).
For all plots, error bars indicate ±SD.

12. Horner, H.A., and Macgregor, H.C. (1983). C value and cell volume: their significance in the evolution and development of amphibians. J. Cell Sci. *63*, 135–146.

13. Cantwell, H., and Nurse, P. (2019). Unravelling nuclear size control. Curr. Genet. *65*, 1281–1285. https://doi.org/10.1007/s00294-019-00999-3.

14. Schmid, M., Evans, B.J., and Bogart, J.P. (2015). Polyploidy in Amphibia. Cytogenet. Genome Res. *145*, 315–330. https://doi.org/10.1159/000431388.

15. Loumont, C., and Kobel, H.R. (1991). *Xenopus longipes* sp. nov., a new polyploid pipid from western Cameroon. Rev. Suisse Zool. *98*, 731–738.

16. Miller, K.E., Brownlee, C., and Heald, R. (2020). The power of amphibians to elucidate mechanisms of size control and scaling. Exp. Cell Res. *392*, 112036. https://doi.org/10.1016/j.yexcr.2020.112036.

17. Michaels, C.J., Tapley, B., Harding, L., Bryant, Z., and Grant, S. (2015). Breeding and rearing the critically cndangered Lake Oku clawed crog (*Xenopus longipes* Loumont and Kobel 1991. Amphib. Rep. Conservator *9*, 100–110.

18. Brown, K.S., Blower, M.D., Maresca, T.J., Grammer, T.C., Harland, R.M., and Heald, R. (2007). *Xenopus tropicalis* egg extracts provide insight into scaling of the mitotic spindle. J. Cell Biol. *176*, 765–770. https://doi.org/10.1083/jcb.200610043.

19. Doherty-Bone, T. (2011). Unravelling the mysteries of Lake Oku, where the frog is "Fon" (king). Froglog *97*, 28–30.

20. Evans, B.J., Carter, T.F., Greenbaum, E., Gvoždík, V., Kelley, D.B., McLaughlin, P.J., Pauwels, O.S.G., Portik, D.M., Stanley, E.L., Tinsley, R.C., et al. (2015). Genetics, morphology, advertisement calls, and historical records distinguish six new polyploid species of African clawed frog (*Xenopus*, *Pipidae*) from West and Central Africa. PLoS One *10*, e0142823. https://doi.org/10.1371/journal.pone.0142823.

21. Newport, J., and Kirschner, M. (1982). A major developmental transition in early *Xenopus* embryos: II. control of the onset of transcription. Cell *30*, 687–696. https://doi.org/10.1016/0092-8674(82)90273-2.

22. Newport, J., and Kirschner, M. (1982). A major developmental transition in early Xenopus embryos: I. characterization and timing of cellular changes at the midblastula stage. Cell *30*, 675–686. https://doi.org/10.1016/0092-8674(82)90272-0.

23. Nieuwkoop, P.D., and Faber, J. (1994). Normal Table of *Xenopus laevis* (Daudin). A Systematical and Chronological Survey of the Development from the Fertilized Egg till the End of Metamorphosis (Garland Science).

24. Chipman, A.D., Khaner, O., Haas, A., and Tchernov, E. (2001). The evolution of genome size: what can be learned from anuran development? J. Exp. Zool. *291*, 365–374. https://doi.org/10.1002/jez.1135.

25. Olmo, E. (1983). Nucleotype and cell size in vertebrates: a review. Basic Appl. Histochem. *27*, 227–256.

26. Olmo, E., Capriglione, T., and Odierna, G. (1989). Genome size evolution in vertebrates: trends and constraints. Comp. Biochem. Physiol. B *92*, 447–453. https://doi.org/10.1016/0305-0491(89)90115-6.

27. Heasman, J. (2006). Patterning the early *Xenopus* embryo. Development *133*, 1205–1217. https://doi.org/10.1242/dev.02304.

28. Edelstein, A.D., Tsuchida, M.A., Amodaj, N., Pinkard, H., Vale, R.D., and Stuurman, N. (2014). Advanced methods of microscope control using μManager software. J. Biol. Methods *1*, 10. https://doi.org/10.14440/jbm.2014.36.

29. Heijo, H., Shimogama, S., Nakano, S., Miyata, A., Iwao, Y., and Hara, Y. (2020). DNA content contributes to nuclear size control in *Xenopus laevis*. Mol. Biol. Cell *31*, 2703–2717. https://doi.org/10.1091/mbc.E20-02-0113.

30. Levy, D.L., and Heald, R. (2010). Nuclear size is regulated by importin α and Ntf2 in *Xenopus*. Cell *143*, 288–298. https://doi.org/10.1016/j.cell.2010.09.012.

31. Jevtić, P., and Levy, D.L. (2015). Nuclear size scaling during Xenopus early development contributes to midblastula transition timing. Curr. Biol. *25*, 45–52. https://doi.org/10.1016/j.cub.2014.10.051.

32. Good, M.C., Vahey, M.D., Skandarajah, A., Fletcher, D.A., and Heald, R. (2013). Cytoplasmic volume modulates spindle size during embryogenesis. Science *342*, 856–860. https://doi.org/10.1126/science.1243147.

33. Gerhart, J.C. (1980). Mechanisms regulating pattern formation in the amphibian egg and early embryo. Biol. Regul. Dev. *3*, 133–316. https://doi.org/10.1007/978-1-4684-9933-9_4.

34. Edgar, B.A., Kiehle, C.P., and Schubiger, G. (1986). Cell cycle control by the nucleo-cytoplasmic ratio in early *Drosophila* development. Cell *44*, 365–372. https://doi.org/10.1016/0092-8674(86)90771-3.

35. Clute, P., and Masui, Y. (1995). Regulation of the appearance of division asynchrony and microtubule-dependent chromosome cycles in *Xenopus laevis* embryos. Dev. Biol. *171*, 273–285. https://doi.org/10.1006/dbio.1995.1280.

36. Session, A.M., Uno, Y., Kwon, T., Chapman, J.A., Toyoda, A., Takahashi, S., Fukui, A., Hikosaka, A., Suzuki, A., Kondo, M., et al. (2016). Genome evolution in the allotetraploid frog *Xenopus laevis*. Nature *538*, 336–343. https://doi.org/10.1038/nature19840.

37. Owens, N.D.L., Blitz, I.L., Lane, M.A., Patrushev, I., Overton, J.D., Gilchrist, M.J., Cho, K.W.Y., and Khokha, M.K. (2016). Measuring absolute RNA copy numbers at high temporal resolution reveals transcriptome kinetics in development. Cell Rep. *14*, 632–647. https://doi.org/10.1016/j.celrep.2015.12.050.

38. Collart, C., Allen, G.E., Bradshaw, C.R., Smith, J.C., and Zegerman, P. (2013). Titration of four replication factors is essential for the *Xenopus laevis* midblastula transition. Science *341*, 893–896. https://doi.org/10.1126/science.1241530.

39. Amodeo, A.A., Jukam, D., Straight, A.F., and Skotheim, J.M. (2015). Histone titration against the genome sets the DNA-to-cytoplasm threshold for the *Xenopus* midblastula transition. Proc. Natl. Acad. Sci. USA *112*, E1086–E1095. https://doi.org/10.1073/pnas.1413990112.

40. Jukam, D., Kapoor, R.R., Straight, A.F., and Skotheim, J.M. (2021). The DNA-to-cytoplasm ratio broadly activates zygotic gene expression in *Xenopus*. Curr. Biol. *31*, 4269–4281.e8.

41. Syed, S., Wilky, H., Raimundo, J., Lim, B., and Amodeo, A.A. (2021). The nuclear to cytoplasmic ratio directly regulates zygotic transcription in Drosophila through multiple modalities. Proc. Natl. Acad. Sci. USA *118*, https://doi.org/10.1073/pnas.2010210118.

42. Nguyen, T., Costa, E.J., Deibert, T., Reyes, J., Keber, F.C., Tomschik, M., Stadlmeier, M., Gupta, M., Kumar, C.K., Cruz, E.R., et al. (2022). Differential nuclear import sets the timing of protein access to the embryonic genome. Nat. Commun. *13*, 5887. https://doi.org/10.1038/s41467-022-33429-z.

43. O'Farrell, P.H. (2015). Growing an embryo from a single cell: a hurdle in animal life. Cold Spring Harb. Perspect. Biol. *7*, a019042. https://doi.org/10.1101/cshperspect.a019042.

44. Brownlee, C., and Heald, R. (2019). Importin α partitioning to the plasma membrane regulates intracellular scaling. Cell *176*, 805–815.e8. https://doi.org/10.1016/j.cell.2018.12.001.

45. Crowder, M.E., Strzelecka, M., Wilbur, J.D., Good, M.C., von Dassow, G., and Heald, R. (2015). A comparative analysis of spindle morphometrics across metazoans. Curr. Biol. *25*, 1542–1550. https://doi.org/10.1016/j.cub.2015.04.036.

46. Wühr, M., Freeman, R.M., Presler, M., Horb, M.E., Peshkin, L., Gygi, S.P., and Kirschner, M.W. (2014). Deep proteomics of the *Xenopus laevis* egg using an mRNA-derived reference database. Curr. Biol. *24*, 1467–1475. https://doi.org/10.1016/j.cub.2014.05.044.

47. Vargas, A., and del Pino, E.M. (2017). Analysis of cell size in the gastrula of ten frog species reveals a correlation of egg with cell sizes, and a conserved pattern of small cells in the marginal zone. J. Exp. Zool. B Mol. Dev. Evol. *328*, 88–96. https://doi.org/10.1002/jez.b.22685.

48. Fankhauser, G. (1945). Maintenance of normal structure in heteroploid salamander larvae, through compensation of changes in cell size by adjustment of cell number and cell shape. J. Exp. Zool. *100*, 445–455. https://doi.org/10.1002/jez.1401000310.

49. Cadart, C., Bartz, J., Oaks, G., Liu, M., and Heald, R. (2022). Ploidy modulates cell size and metabolic rate in *Xenopus* embryos. Preprint at bioRxiv. https://doi.org/10.1101/2022.10.17.512616.

50. Scott, M., Gunderson, C.W., Mateescu, E.M., Zhang, Z., and Hwa, T. (2010). Interdependence of cell growth and gene expression: origins and consequences. Science *330*, 1099–1102. https://doi.org/10.1126/science.1192588.

51. Vinogradov, A.E., and Anatskaya, O.V. (2006). Genome size and metabolic intensity in tetrapods: a tale of two lines. Proc. Biol. Sci. *273*, 27–32. https://doi.org/10.1098/rspb.2005.3266.

52. Molenaar, D., Van Berlo, R., De Ridder, D., and Teusink, B. (2009). Shifts in growth strategies reflect tradeoffs in cellular economics. Mol. Syst. Biol. *5*, 323. https://doi.org/10.1038/msb.2009.82.

53. Schindelin, J., Arganda-Carreras, I., Frise, E., Kaynig, V., Longair, M., Pietzsch, T., Preibisch, S., Rueden, C., Saalfeld, S., Schmid, B., et al. (2012). Fiji: an open-source platform for biological-image analysis. Nat. Methods *9*, 676–682. https://doi.org/10.1038/nmeth.2019.

54. Edelstein, A.D., Tsuchida, M.A., Amodaj, N., Pinkard, H., Vale, R.D., and Stuurman, N. (2014). Advanced methods of microscope control using mManager software. J. Biol. Methods *1*, 10.

55. Lee, C., Kieserman, E., Gray, R.S., Park, T.J., and Wallingford, J. (2008). Whole-mount fluorescence immunocytochemistry on *Xenopus* embryos. CSH Protoc. *2008*. pdb.prot4957. https://doi.org/10.1101/pdb.prot4957.

STAR★METHODS

KEY RESOURCES TABLE

REAGENT or RESOURCE	SOURCE	IDENTIFIER
Antibodies		
Rabbit anti-Histone H3	Abcam	Cat#: ab1791; RRID: AB_302613
Mouse anti-Beta-tubulin E7	Developmental Studies Hybridoma Bank	Cat#: E7; RRID: AB_2315513
Mouse anti-ZO-1 (ZO-1A12)	Thermo Fisher	Cat # 33-9100; RRID: AB_2533147
Rabbit anti-Phospho-Histone H3 [pSer10]	Millipore Sigma	Product # 06-570; RRID: AB_310177
Alexa Fluor 488	Invitrogen	Cat#: A-11008; RRID: AB_143165
Alexa Fluor 568	Invitrogen	Cat#: A-11011; RRID: AB_143157
Biological samples		
Adult *Xenopus paratropicalis* blood smears	Ben Evans, McMaster University	N/A
Chemicals, peptides, and recombinant proteins		
Pregnant mare serum gonadotrophin	Calbiochem	Cat#: 367222
Human chorionic gonadotrophin	Sigma Aldrich	Cat#: CG10
Giemsa stain	Sigma Aldrich	Product # R03055
Experimental models: Organisms/strains		
Xenopus laevis	Nasco	Cat#: LM00535
Xenopus laevis	National Xenopus Resource	Cat#: NXR_0031
Xenopus tropicalis	Nasco	Cat#: LM00822
Xenopus tropicalis	National Xenopus Resource	Cat#: NXR_1018
Xenopus borealis	Nasco	Cat#: LM00698
Xenopus longipes	California Academy of Sciences (San Francisco, CA, USA)	N/A
Hymenochirus boettgeri	Albany Aquarium (Albany, CA, USA)	N/A
Software and algorithms		
FIJI	Schindelin et al.[53]	https://imagej.net/software/fiji/
Matlab	N/A	https://www.mathworks.com/products/matlab.html
GraphPad Prism	N/A	https://www.graphpad.com/scientific-software/prism/
Cell and nuclear volume measurement macro for Fiji	N/A	https://visikol.com/wp-content/uploads/2019/02/Visikol-Measure-Volume-Macro.ijm

RESOURCE AVAILABILITY

Lead contact

Further information and requests for resources and reagents should be directed to and will be fulfilled by the lead contact, Rebecca Heald (bheald@berkeley.edu).

Materials availability

This study did not generate new unique reagents.

Data and code availability

- Images and measurement data reported in this paper will be shared by the lead contact upon request.
- This paper does not report original code.
- Any additional information required to reanalyze the data reported in this paper is available from the lead contact upon request.

EXPERIMENTAL MODEL AND SUBJECT DETAILS

All frogs were used and maintained in accordance with standards established by the UC Berkeley Animal Care and Use Committee and approved in our Animal Use Protocol. Mature *Xenopus laevis*, *X. tropicalis*, and *X. borealis* frogs were obtained from Nasco (Fort Atkinson, WI) or the National *Xenopus* Resource (Woods Hole, MA). Mature *X. longipes* frogs were obtained from California Academy of Sciences (San Francisco, CA). Mature *H. boettgeri* frogs were obtained from Albany Aquarium (Albany, CA).

All frogs were housed in a recirculating tank system with regularly monitored temperature and water quality (pH, conductivity, and nitrate/nitrite levels). *X. laevis* and *X. borealis* were housed at 20–23°C, *X. tropicalis* were housed at 23-26°C, and *X. longipes* were housed at 19-21°C. *H. boettgeri* were housed at 20-23°C. All animals were fed Nasco frog brittle. *X. longipes* were supplemented twice weekly with frozen/thawed bloodworms (Chironomidae).

Chemicals

Unless otherwise stated, all chemicals were purchased from Sigma-Aldrich, St. Louis, MO.

Frog care

X. laevis and *X. tropicalis*, and females were ovulated with no harm to the animals with a 6-and 3-month rest interval, respectively. To obtain testes for in vitro fertlizations in *X. laevis* and *X. tropicalis*, males were euthanized by over-anesthesia through immersion in ddH2O containing 0.15% MS222 (Tricaine; Sigma) neutralized with 5 mM sodium bicarbonate prior to dissection, and then frozen at -20°C. Tadpoles used for experiments were euthanized similarly prior to fixation.

Natural matings were stimulated in *X. longipes* with no harm to males or females with a 4-6 month rest interval.

METHOD DETAILS

Erythrocyte preparation and measurements

A small drop of blood was collected from the frog foot of each species with a sterile needle, and the drop was smeared on a slide. The smear was then fixed with methanol and stained with Giemsa stain (Sigma). Cells were imaged in brightfield using Micromanager software[54] with an upright Olympus BX51 microscope equipped with a Olympus UPlan 40x air objective and ORCA-II camera (Hamamatsu Photonics). Cross-sectional areas of cells and nuclei were measured in Fiji[53] using the freehand tool. *X. paratropicalis* blood smears were a kind gift from Ben Evans (McMaster University).

Epithelial cell preparation and measurements

Shed frog skin was collected from frog housing tanks and mounted carefully on a microscope slide by rolling the skin flat so that a monolayer of cells could be imaged. Cells were imaged immediately after collection, unstained and without a coverslip, in brightfield using Olympus cellSens Dimension 2 software on an upright Olympus BX51 microscope equipped with an ORCA-II camera (Hamamatsu Photonics) and an Olympus UPlan 20x air objective. Cross sectional areas of cells and nuclei were measured in Fiji using the freehand tool.

Natural mating of *X. longipes*

X. longipes were a kind gift from California Academy of Sciences. Male and female *X. longipes* were injected with a priming dose of 75 IU HCG (Sigma) 48 hours before the desired mating day, and kept separately to avoid premature amplexus. On the day of ovulation, males and females were injected with a boosting dose of 200 IU HCG. Amplexus began soon after injection with egg laying 6-8 hours later. Embryos were collected in batches for fixation and live imaging.

In vitro fertilization of *X. laevis*

X. laevis females were primed with 100 IU of pregnant mare serum gonadotropin (PMSG, Calbiochem) at least 48 h before use and boosted with 500 IU of HCG (Human Chorionic Gonadotropin CG10, Sigma) 14-16 hours before experiments. To obtain testes, males were euthanized by anesthesia through immersion in double-distilled (dd)H2O containing 0.15% MS222 (tricaine) neutralized with 5 mM sodium bicarbonate before dissection. Testes were collected in 1X Modified Ringer (MR) (100 mM NaCl, 1.8 mM KCl, 1 mM MgCl2, 5 mM HEPES-NaOH pH 7.6 in ddH2O) and stored at 4°C until fertilization. To prepare the sperm solution, 1/3 testis was added to 1 mL of ddH2O in a 1.5 mL microcentrifuge tube, and homogenized using scissors and a pestle. *X. laevis* females were squeezed gently to deposit eggs onto petri dishes coated with 1.5% agarose in 1/10X MMR (1X MMR: 100 mM NaCl, 2 mM KCl, 2 mM CaCl2, 1 mM MgSO4, 0.1 mM EDTA, 5 mM HEPES-NaOH pH 7.6 in ddH2O). Any liquid in the petri dishes was removed and the eggs were fertilized with 1 mL of sperm solution per dish. Fertilized embryos were swirled in the solution to form a monolayer on the bottom of the petri dish and incubated for 10 min with the dish slanted to ensure submersion of eggs. Dishes were then flooded with 1/10X MMR, swirled and incubated for 10 min. To remove egg jelly coats, the 1/10X MMR was completely exchanged for freshly prepared Dejellying Solution (2% L-cysteine in ddH2O-NaOH, pH 7.8). After dejellying, eggs were washed extensively (>4X) with 1/10X MMR before incubation at 23°C. At Nieuwkoop and Faber stage 2-3, fertilized embryos were sorted and placed in fresh 1/10X MMR in new petri dishes coated with 1.5% agarose in 1/10X MMR.

Please cite this article in press as: Miller et al., Dodecaploid *Xenopus longipes* provides insight into the emergence of size scaling relationships during development, Current Biology (2023), https://doi.org/10.1016/j.cub.2023.02.021

CellPress
OPEN ACCESS

Maintenance of *Xenopus* embryos

X. laevis, *tropicalis*, and *longipes* embryos were raised side by side in 1.5% agarose in 1/10X MMR -coated petri dishes covered in 1/10X MMR in a 23 °C incubator. The MMR was changed and dead/lysed embryos removed frequently to prevent contamination.

Imaging and measurement of egg diameters, developing embryos, and tadpoles

For still images, eggs and embryos were placed in an agarose-coated imaging chamber filled with a limited amount of 1/10X MMR to prevent depth-biased measurements and imaged at 12x-31x magnification using a Wild Heerbrugg M7A StereoZoom microscope coupled to a Leica MC170HD camera and Leica LAS X software. Diameter of eggs was measured using the line tool in Fiji.

Live imaging

Movies of Xenopus embryo development were made by placing embryos in 1/10X MMR in imaging dishes prepared using an in-house PDMS mold designed to create a pattern of 1.5 mm large wells in agarose that allowed us to image embryos of each species simultaneously. Time-lapse movies of animal poles were acquired at 6-10x magnification using a Zeiss Discovery V8 stereoscope coupled to a Leica DMC2900 camera and Leica LAS X software. Images were acquired either at a frequency of one frame every 10 s for 20 h, or one frame every 4 minutes for 15-30 hours. Movies are compressed to 15 frames per second.

Cell Cycle Duration measurement

Cell cycles were measured as described in Amodeo et al.[39] Movies were started at ~2 h post-fertilization (after the first or second cleavage). Embryos were allowed to develop in 1/10X MMR. Divisions were counted to determine the frame number of each cleavage. Then, ~3 individual cells were selected from the visible portion of each embryo after the eighth cleavage. The period between cleavages was determined by manually tracking individual cells and noting the frame number at which the cleavage furrow visibly transected the entire cell. When daughter cells did not divide concurrently, the division time of the earliest dividing daughter was always used, and that cell was followed for the remainder of the movie. When the cleavage could not be observed, as in cases where the cleavage plane did not intersect the embryo surface, the cell was omitted from analysis.

P-values were calculated using a two-tailed t-test with unequal variance between the indicated distributions. At least 3 cells were counted for each embryo at each cell cycle using 10 total embryos from 3 separate clutches.

Embryo whole mount immunofluorescence

To label nuclei, cell borders, and mitotic/meiotic spindles, embryos at the desired developmental stage were fixed for one hour using MAD fixative (2 parts methanol [Thermo Fisher Scientific], 2 parts acetone [Thermo Fisher Scientific]), 1 part DMSO [Sigma]). After fixation, embryos were dehydrated in methanol and stored at -20°C. Embryos were then processed as previously described[55] with modifications. Following gradual rehydration in 0.5X SSC (1X SSC: 150 mM NaCl, 15 mM Na citrate, pH 7.0), embryos were bleached with 1-2% H_2O_2 (Thermo Fisher Scientific) in 0.5X SSC containing 5% formamide (Sigma) for 2-3 h under light, then washed in PBT (137 mM NaCl, 2.7 mM KCl, 10 mM Na_2HPO_4, 0.1% Triton X-100 [Thermo Fisher Scientific]) and 2 mg/mL bovine serum albumin (BSA). Embryos were blocked in PBT supplemented with 10% goat serum (Thermo Fisher Scientific) and 5% DMSO for 1-3 h and incubated overnight at 4°C in PBT supplemented with 10% goat serum and primary antibodies. The following antibodies were used to label tubulin, tight junctions, DNA, and Phospho-histone H3: 1:250 mouse anti-beta tubulin (E7; Developmental Studies Hybridoma Bank, Iowa City, IA), 1:1000 mouse anti-ZO-1(ZO-1A12; Thermo Fisher Scientific), 1:250 rabbit anti-histone H3 (ab1791; Abcam), 1:1000 Anti-phospho-Histone-H3(ser10) (06-570; Sigma). Embryos were then washed 4× 2 h in PBT and incubated overnight in PBT supplemented with 1:500 goat anti-mouse or goat anti-rabbit secondary antibodies coupled either to Alexa Fluor 488 or 568 (Thermo Fisher Scientific). Embryos were then washed 4× 2 h in PBT and gradually dehydrated in methanol. Embryos were cleared in Murray's clearing medium (2 parts of Benzyl Benzoate [Sigma], 1 part of Benzyl Alcohol [Sigma]).

Confocal imaging and measurement of embryos, cells and nuclei after whole mount immunofluorescence

Embryos were placed in a reusable AttoFluor Cell Chamber (Thermo Fisher Scientific A7816) in fresh Murray's clearing medium for confocal microscopy. Confocal microscopy was performed on a Zeiss LSM 800 confocal running the Zeiss Zen Software. Embryos were imaged using a Plan-Achromat 20x/0.8 air objective and laser power of 0.5-2%, on multiple 1024x1024 pixel plans spaced 0.68-1.2 μm apart in Z. In stage 8 embryos, before differentiation, we measured an equal distribution of both animal and vegetal cells closest to the surface of the embryo, where staining was most penetrant. In stage 21, 36, and 48 embryos, we measured both ciliated and unciliated cells of the surface epithelium. Cross-sectional areas of cells and nuclei were measured in Fiji at the central plane of the cell or nucleus using the freehand tool.

Egg volume and N/C ratio calculations

Egg volume was calculated from 2D stereo images of eggs from each species as described above in "Imaging and measurement of egg diameters, developing embryos, and tadpoles". The diameter of each egg was measured using the line tool in Fiji and the volume calculated using the formula for volume of a sphere ($V = 4/3\ \pi r^3$). N/C ratios in Figures 3H and S3H were extrapolated from 2D cross-sectional area measurements using a method described and validated for embryos ≥ stage 8.[30–32] The cross- sectional area of the nucleus at its widest part was divided by the cross-sectional area of the cell at the same location in Z, then multiplied by 100 to express N/C volume ratio as a percent. This method closely approximated cell and nuclear volume measurements made using 3D reconstructions of our confocal Z-stacks (Figure S3G), analyzed by a macro for Fiji (available at https://visikol.com/wp-content/uploads/2019/02/Visikol-Measure-Volume-Macro.ijm).

QUANTIFICATION AND STATISTICAL ANALYSIS

Box plots were generated in Matlab (Figures 1E, 1G, and 1H) or using GraphPad Prism software (all others) which plot the mean and standard deviation for each condition. Statistical parameters for each experiment (ie exact value of n, what n represents, means and standard deviations) are reported in the figure legends. P-values between pairwise averages were generated using a two-tailed student's t-test. Simple linear regression plots (i.e. In Figures 2C, 2D, and 3D–3F) were generated using GraphPad Prism software, which calculated the Pearson's Correlation Coefficient (R), trendline for regression (R^2), and Slope Coefficient for each trendline.